scientific reports

Check for updates

OPEN

Utilization of Galerkin finite element strategy to investigate comparison performance among two hybrid nanofluid models

Muhammad Sohail[1]✉, Umar Nazir[2], Samaira Naz[3], Abha Singh[4], Kanit Mukdasai[2]✉, Mohamed R. Ali[5,6]✉, Muhammad Jahangir Khan[7] & Ahmed M. Galal[8,9]

The utilization of Fourier's law of heat conduction provides the parabolic partial differential equation of thermal transport, which provides the information regarding thermal transport for the initial time, but during many practical applications, this theory is not applicable. Therefore, the utilization of modified heat flux model is to be used. This work discusses the utilization of non-Fourier heat flux model to investigate thermal performance of tri-hybrid nanoparticles mixture immersed in Carreau Yasuda material past over a Riga plate by using Hamilton Crosser and Yamada Ota models considering the variable thermos-physical characteristics. The phenomenon presenting the transport of momentum and energy are developed in the form of coupled partial differential equations, which are complex and then transformed into ordinary differential equations by using an appropriate transformation. The transformed equations have been tackled numerically via finite element scheme and the authenticity of obtained solution is shown with the help of comparative analysis of present results with those are available in open literature.

Abbreviations

V_1, V_2	Velocity components
G	Gravitational acceleration
ρ	Fluid density
d	Fluid number
C_p	Specific heat
T_∞	Ambient temperature
Γ	Fluid number
c	Stretching number
u_w	Wall velocity
T_w	Wall temperature
ODEs	Ordinary differential equation
hybrid	Hybrid nanofluid
bf, f	Base fluid and fluid

[1]Department of Mathematics, Khwaja Fareed University of Engineering and Information Technology, Rahim Yar Khan 64200, Pakistan. [2]Department of Mathematics, Faculty of Science, Khon Kaen University, Khon Kaen 40002, Thailand. [3]Department of Mathematics, Government College University, Faisalabad, Pakistan. [4]Department of Basic Science, College of Science and Theoretical Study, Dammam-Female Branch, Saudi Electronic University, Riyadh, Saudi Arabia. [5]Faculty of Engineering and Technology, Future University in Egypt, New Cario 11835, Egypt. [6]Basic Engineering Science Department, Benha Faculty of Engineering, Benha University, Benha, Egypt. [7]Department of Advance Materials and Technologies, Faculty of Materials Engineering, Silesian University of Technology, 44-100 Gliwice, Poland. [8]Mechanical Engineering Department, College of Engineering, Prince Sattam Bin Abdulaziz University, Wadi Addawaser 11991, Saudi Arabia. [9]Production Engineering and Mechanical Design Department, Faculty of Engineering, Mansoura University, P.O 35516, Mansoura, Egypt. ✉email: muhammad_sohail111@yahoo.com; kanit@kku.ac.th; mohamed.reda@fue.edu.eg

H_t	Heat source number
Re	Reynolds number
Q, q_m	Wall heat flux and wall mass flux
β_a	Time relaxation parameter
∞	Infinity
F	Dimensionless velocity
s_1, s_2	Solid particles
w_2, w_1, w_3	Weight functions
η	Independent variable
E, θ_γ	Energy and variable viscosity parameter
SiO_2	Silicon dioxide
L	Length of cylindrical particles
y, x	Space coordinates
β_1	Coefficient of thermal and solute concentration
M_0, J_0	Electromagnetic force components
Q_0	Heat source
T	Fluid temperature
k	Thermal conductivity
K_M	Chemical reaction
η	Independent parameter
ν_∞	Kinematic viscosity from away of surface
ϵ_1	Thermal conductivity and mass diffusion coefficients
We	Wiesenberger number
λ_1	Bouncy parameters
θ	Dimensionless temperature
ϕ_1	Volume fractions
Pr	Prandtl number
Cf	Skin friction coefficient
Nu	Nusselt number
μ	Kinematic viscosity
FEM	Finite element method
BCs	Boundary conditions
ω	Electromagnetic magnetic force parameter
PDEs	Partial differential equations
ψ_j	Shape function
TiO_2	Titanium dioxide
$C_2H_6O_2$	Ethylene glycol
D	Diameter of cylindrical particles

Industrial applications for hybrid nanofluids are still in the early stages of development. Hybrid nanofluids have only recently emerged as a new phenomenon, even though nanofluids have existed for decades. Hybrid nanofluids are expected to improve current application performance levels. A handful of hybrid nanofluid applications are currently being researched. They are expected to have the same density, heat capacity, and viscosity as their mono-component counterparts. The heat transfer coefficient can be significantly increased when two or more nanofluids are mixed. Researchers' interest in hybrid nanofluid applications has recently been piqued. Thermal storage, welding lubrication, transformer cooling, refrigeration, and biomedical and drug-reduction heat pipe cooling have many applications. The following are other potential uses: magnetic nanofluids have been used in various applications by researchers. Using a magnetic field can improve their ability to transfer heat.

It is possible to achieve thermal equilibrium with a wide variety of liquids. Fourier's law ignores the liquid's thermal relaxation characteristics when calculating heat transfer. The Fourier law makes it challenging to model heat transfer in fluids. These two scientists came up with a new heat conduction theory to solve this problem. Researchers came up with a new Fourier law for heat transfer in response to this new theory. Researchers frequently make use of these principles. Regardless of the outcome, our research is essential and must be completed. Reddy et al.[1] estimated thermal enactment of hybrid nanoparticles in bio-magnetic pulsatile considering nanofluid in irregular channel. Xiu et al.[3] discussed impacts of tri-hybrid nanoparticles in Reiner Philippoff liquid considering non-uniform Lorentz force past a stretching surface. They have adopted FEM to conduct numerical consequence and estimated comparison among hybrid nanoparticles and tri-hybrid nanoparticles. They have included that thermal enhancement for tri-hybrid nanofluid is better than thermal performance for hybrid nanoparticles. A study by Dogonchi and colleagues[4] investigated the effect of nanoparticles on fluid heat transfer. They have used heat transfer theory to determine the thermal relaxation time. Al-Mdallal et al.[5] visualized entropy optimization in pseudoplastic nano-polymer in occurrence of Lorentz force past a circular cylinder. Basha et al.[6] utilized finite element method to obtain results of bio fluid associated with hybrid nanofluid in the presence of Lorentz force in stenosis artery. Reddy et al.[7] performed role of entropy generation in peristaltic fluid considering nanofluid based on gold-blood in a microchannel. Basha and Sivaraj[8] discussed results of entropy generation in Eyring–Powell fluid in the presence of biomedical applications in heated channel. In addition, it appears that numerous relevant works[9–12] have been cited as well.

The heat transfer mechanisms are strikingly similar to those governing solute distribution in liquids. To incorporate the generalized Fourier heat transfer law into Fick's equations, scientists had to conduct prior research on

the Fick law and the generalized Fourier heat transfer law. Fick's law of mass and heat transfer in Prandtl fluids is the focus of this study (non- Newtonian fluid). The current investigation will be better positioned if prior studies are reviewed. In the presence of nanoparticles, thermal transport is significantly accelerated. According to Haneef and colleagues[13], the Cattaneo-Christov rheological fluid has heat and mass flux. Nawaz et al.[14] studied the temperature-dependent coefficients of viscoelastic fluids using a theory other than the Fourier transform. The thermal act of a micro-polar fluid with monocity and hybridity was evaluated by Nawaz and his colleagues using a novel heat flux theory.

Recent years have seen a rise in interest in fluids that can be used in various industrial and domestic contexts. The list includes ink, nail polish, ketchup, and even wall paint. On the condiment bar, ketchup and whipped cream are included. Shear-thinning, pseudo-plastic, and plastic fluid are all terms that can be used interchangeably. As a result of the shear-thinning effect, fluids flow more easily under shear-thinning stresses. Oil paint, cream, and other mediums can benefit significantly from this feature. In a team led by Eberhard, The power law theory was used for the first time to calculate an effective shear rate. They went into the study assuming that the permeability would remain constant. Materials were subjected to shear thickening and thinning tests by Rosti and Takagi. A wide range of distinctive features was thus discovered. Gul et al.[15] solved the thin-film power-law model for slip lifting and drainage. Sketches and various fluid velocity parameters were used to estimate the flow rate and coefficient of skin friction. The slip parameter was found to increase with a decrease in velocity. Hussein et al. investigated Brownian motion and thermophoresis in nanofluids in a vertical cylinder apparatus. Curvature calculations on the fluid and the model were used to determine the speed reductions. Abdelsalam and Sohail[16] found that bioconvection affects the flow of nanofluids with varying viscosities over an elongated bidirectional surface. It was discovered that the motile density profile and the Peclet and Lewis indices were linked. Brownian motion and time-dependent thermophoresis can be used to study the thermal and concentration relaxation times of Sutterby flows. With the help of boundary layer theory and a suitable similarity transformation, they were able to turn the physical model into a coupled PDE system (PDEs). As a result of this update, the model can now be used to investigate a broader range of physical phenomena. After the ODEs had been converted, they were examined. The Prandtl number was used to gauge the temperature. The Schmidt number was increased by increasing the solution's concentration. In Chu and colleagues[17], activation energy and chemical reactions significantly impact nanofluid flow. There was a decrease in fluid velocity when the Keller box scheme was implemented. Basha and Sivaraj[18] evaluated features of entropy generation inserting Fe_3O_4-blood nanofluid in porous surface. In the case of pseudo-plastic drainage and lifting, the relationship between velocity decrease and Stokes number established by Alam et al.[19] can be used to solve the problem. The pseudo-plastic model with variable viscosity showed flow. This paragraph necessitates citations. A perturbation technique was used to increase the magnetic parameter value and the velocity to solve the boundary value problem. New parameters have also been added to the studies conducted in[20–22,29–31] and references therein.

Physical aspects of flow model

Two dimensional model regarding rheology of Carreau Yasuda martial is developed and flowing assumptions are observed as

- Vertical Riga plate is considered;
- Two dimensional and incompressible flow are assumed;
- Heat generation and variable thermal conductivity are adopted;
- The suspension of (TiO_2/SiO_2) in ethylene glycol is inserted;
- Lorentz force and bouncy forces are addressed;
- Two kinds of nanomaterial in EG (ethylene glycol) are imposed;
- Non-Fourier's law is utilized;
- Hamilton Crosser and Yamada Ota models are imposed;
- Variable fluidic properties are addressed;
- The graphical representations of geometry are mentioned by Fig. 1.

Figure 1 shows a vertical surface and Riga plate. It is mentioned that y-axis is considered as horizontal and x-direction is assumed as a vertical direction. The constant magnetic field is inserted along y-direction whereas Riga plate is considered under electromagnetic force. Momentum and thermal boundary layers are generated. The motion of tri-hybrid nanoparticles is induced using wall velocity (u_w). The desired PDEs[23,24] are obtained as

$$\frac{\partial V_1}{\partial x} + \frac{\partial V_2}{\partial y} = 0, \tag{1}$$

$$V_1\frac{\partial V_1}{\partial x} + V_2\frac{\partial V_1}{\partial y} = \frac{G(\beta_2)_{hybrid}(T - T_\infty)}{\rho_{hybrid}} + \frac{M_0\pi j_0}{8\rho_{hybrid}}exp\left(-\frac{\pi}{a}y\right) + \frac{\partial}{\partial y}\left[\mu^{\theta}_{hybrid}\left\{1 + \Gamma^d\left(\left(\frac{\partial V_1}{\partial y}\right)^d\right)^{\left(\frac{n-1}{d}\right)}\right\}\frac{\partial V_1}{\partial y}\right], \tag{2}$$

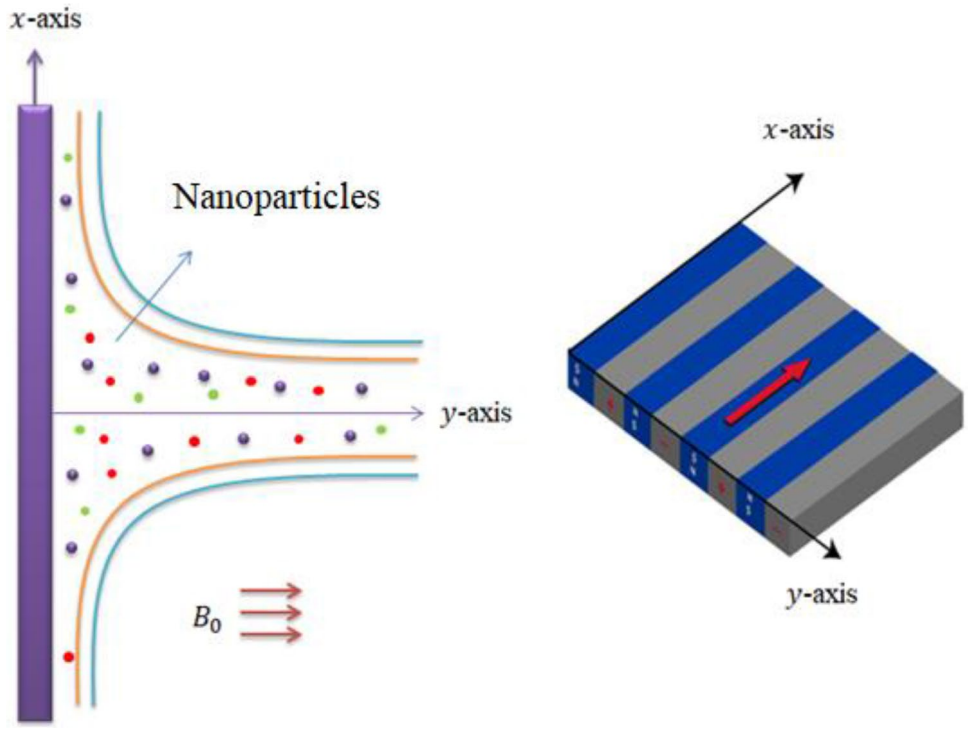

Figure 1. Geometry and coordinates system.

$$V_1\frac{\partial T}{\partial x}+V_2\frac{\partial T}{\partial y}+\gamma_1\left[\begin{array}{c}V_1^2\frac{\partial^2 T}{\partial x^2}+V_2^2\frac{\partial^2 T}{\partial y^2}+2V_1V_2\frac{\dot{\partial} T}{\partial x\partial y}+\left(V_1\frac{\partial V_1}{\partial x}+V_2\frac{\partial V_1}{\partial x}\right)\frac{\partial T}{\partial x}\\+\left(V_1\frac{\partial V_2}{\partial x}+V_2\frac{\partial V_2}{\partial x}\right)\frac{\partial T}{\partial y}-\frac{Q_0}{(\rho C_p)_{hnf}}\left(V_1\frac{\partial T}{\partial x}+V_2\frac{\partial T}{\partial y}\right)\end{array}\right]$$
$$=\frac{1}{(\rho C_p)_{hybrid}}\frac{\partial}{\partial y}\left(k^T_{hybrid}\frac{\partial T}{\partial y}\right)-\frac{Q_0}{(\rho C_p)_{hybrid}}(T-T_\infty). \tag{3}$$

BCs[23,24] are

$$u_w=cx=V_1, V_2=0, T=T_w, y:=0, V_1\to 0, T\to T_\infty : y\to\infty. \tag{4}$$

The desire transformations[23] are delivered as

$$\eta=y\left(\frac{u_w}{x\nu_\infty}\right)^{\frac{1}{2}}, \frac{T-T_\infty}{T_w-T_\infty}=\theta, V_1=cxF', V_2=-\sqrt{c\nu_f}F. \tag{5}$$

Thermal condictivity in term of variable form[2] which are

$$k^t_{hybrid}=k_{hybrid}\left[1+\epsilon_1\left(\frac{T-T_\infty}{T_w-T_\infty}\right)\right], \frac{1}{\mu^\theta_{hybrid}}=\frac{1+\gamma(T-T_\infty)}{\mu_{hybrid}}. \tag{6}$$

ODEs are achieved using Eq. (6) and obtained as

$$\frac{\theta_\gamma}{(\theta_\gamma-1)^2}\left\{1+(d+1)nWe^dF''^2\right\}^{\frac{n-1}{d}}F''\theta'+\frac{\nu_f}{\nu_{hybrid}}\left(FF''-F'F'\right)+\frac{\nu_f}{\nu_{hybrid}}\lambda_1\theta$$
$$+\frac{\omega exp}{A_1}(-\eta\beta)++\frac{\theta_\gamma}{\theta_\gamma-1}\left\{1+(d+1)nWe^dF''^2\right\}\left\{1+(d+1)nWe^dF''^2\right\}^{\frac{n-3}{d}}F'''=0, \tag{7}$$

$$(1+\epsilon_1\theta)\theta''+\epsilon_1(\theta')^2-\beta_a\,\mathrm{Pr}\,\frac{k_f(\rho C_p)_{hybrid}}{k_{hybrid}(\rho C_p)_f}\left(FF'\theta'+F^2\theta''+H_tF\theta'\right)+\frac{k_f}{k_{hybrid}}\mathrm{Pr}\,H_t\theta$$
$$+\frac{k_f(\rho C_p)_{hybrid}}{k_{hybrid}(\rho C_p)_f}\mathrm{Pr}\,F\theta'=0. \tag{8}$$

	K	C_p	ρ
$C_2H_6O_2$	0.253	2430	1113.5
TiO_2	8.4	692	4230
SiO_2	1.4013	3.5×10^6	2270

Table 1. Thermal properties[17] of two kinds of nanofluid in EG (ethylene glycol).

Using Eq. (6) in Eq. (5) and BCs are

$$F'(\infty) = 0, \theta(0) = 1, F(0) = 0, F'(0) = 1, \theta(\infty) = 0. \tag{9}$$

The correlations between two kinds of hybrid nanomaterial models[25] are given below and the relationship between the physical quantities is mentioned in Table 1.

$$\left.\begin{array}{c} \rho_{hybrid} = \left[(1-\phi_2)\left\{(1-\phi_1)\rho_f + \phi_1\rho_{s1}\right\}\right] + \phi_2\rho_{s2} \\ \left(\rho C_p\right)_{hybrid} = \left[(1-\phi_2)\left\{\begin{array}{c}(1-\phi_1)\left(\rho C_p\right)_f \\ +\phi_1\left(\rho C_p\right)_{s1}\end{array}\right\}\right] + \phi_1\left(\rho C_p\right)_{s2} \\ \left\{\frac{k_{s1}+(m-1)k_f-(m-1)\phi_1\left(k_f-k_{s2}\right)}{k_{s1}+(m-1)k_f-\phi_1\left(k_{s2}-k_f\right)}\right\} = \frac{k_{bf}}{k_f} \end{array}\right\}, \tag{10}$$

$$\left.\begin{array}{c} \mu_{hybrid} = \frac{(1-\phi_2)^{2.5}\mu_f}{(1-\phi_1)^{2.5}}, \frac{k_{nf}}{k_f} = \left\{\frac{k_s+(m+1)k_f-(m-1)\phi\left(k_f-k_s\right)}{k_s+(m-1)k_f+\phi\left(k_f-k_s\right)}\right\} \\ \frac{k_{hybrid}}{k_{bf}} = \left\{\frac{k_{s2}+(m-1)k_{bf}-(1-m)\phi_2\left(k_{s2}-k_{bf}\right)}{k_{s2}+(m-1)k_{bf}-\phi_2\left(k_{bf}-k_{s2}\right)}\right\} \\ \left\{\frac{k_{s2}+(m-1)k_{bf}-(1-m)\phi_2\left(k_{s2}-k_{bf}\right)}{k_{s2}+(m-1)k_{bf}-\phi_2\left(k_{bf}-k_{s2}\right)}\right\} = \frac{k_{hybrid}}{k_{bf}} \end{array}\right\}, \tag{11}$$

$$\frac{k_{hybrid}}{k_{bf}} = \left\{\begin{array}{c}\left\{\frac{\frac{k_{s2}}{k_{bf}}+\chi+\chi\phi_2\left(1-\frac{k_{s2}}{k_{bf}}\right)}{\frac{k_{s2}}{k_{bf}}+\chi+\phi_2\left(1-\frac{k_{s2}}{k_{bf}}\right)}\right\}, \chi = 2{\phi_2}^{0.2}\frac{L}{D}\ for\ cylindrical\ particle \\ \chi = 2{\phi_2}^{0.2}\ for\ spherical\ particle\end{array}\right\}, \tag{12}$$

$$\frac{k_{bf}}{k_f} = \left\{\begin{array}{c}\left\{\frac{\frac{k_{s1}}{k_f}+\chi+\chi\phi_1\left(1-\frac{k_{s1}}{k_f}\right)}{\frac{k_{s1}}{k_f}+\chi+\phi_1\left(1-\frac{k_{s1}}{k_f}\right)}\right\}, \chi = 2{\phi_2}^{0.5}\frac{L}{D}\ for\ cylindrical\ particle \\ \chi = 2{\phi_2}^{0.5}\ for\ spherical\ particles\end{array}\right\}. \tag{13}$$

Parameters appeared in Eqs. (9)–(12) which are defined as

$$\theta_\gamma = \frac{1}{\gamma(T_w - T_\infty)}, \beta_a = c\gamma_1, We = \frac{\Gamma a\sqrt{a}}{\sqrt{\nu_f}}, Pr = \frac{\left(C_p\right)_f\mu_f}{k_f}, H_t = \frac{\pi M_0 j_0}{\rho_f 8u_w a}, \beta = \left(\frac{\pi^2\nu_f}{ca^2}\right)^{1/2}.$$

Shear stress is defined as

$$Cf = \frac{\tau_w}{(u_w)^2\rho_f}, \tau_w = \mu_{hybrid}\left[\left(1 + \left(\frac{n-1}{d}\right)\Gamma^d\left(\frac{\partial V_1}{\partial y}\right)^d\frac{\partial V_1}{\partial y}\right)\right]_{y=0} \tag{14}$$

Skin friction coefficient and temeprature gradient[23,24] is delievered as

$$Re^{1/2}Cf = -(1-\phi_1)^{-2.5}(1-\phi_2)^{-2.5}\left[1 + \frac{n-1}{d}\left(WeF''(0)\right)^d\right]F''(0), \tag{15}$$

$$Nu = \frac{xQ}{(T-T_\infty)k_f} = -\frac{k_f}{k_{hybrid}Re^{-\frac{1}{2}}}(1+\epsilon_1)\theta'(0), \tag{16}$$

Numerical approach

Finite element apparoch is utlized to find numerical solution of resultant transformed ODEs (ordinary differential equations). Tables 2 and 3 are preapred to estimate grid size study and validation of problem. The proposed methodology is shown with the help of Fig. 2. Several advantages of finite element method are presecribed below.

e	$F'\left(\frac{\eta_{max}}{2}\right)$	$\theta\left(\frac{\eta_{max}}{2}\right)$
30	0.5721974488	0.3921033142
60	0.5460428484	0.3836649886
90	0.5373843928	0.3808296144
120	0.5330677499	0.5076407203
150	0.5304818169	0.5059713564
180	0.5287599374	0.5048579897
210	0.5275304862	0.3775697622
240	0.5266088495	0.5034653655
270	0.5258925734	0.5030028093
300	0.5253200716	0.5026336120

Table 2. Grid size study of concentration, teeprature and velocity for 300 elements when $We = 3.0, d = 1, \lambda_1 = 0.3, \beta = 2.0, \epsilon_1 = 1.4, \beta_a = 0.5, Pr = 206, H_t = -2.0, Sc = 3.0, \phi_1 = 0.004, \phi_2 = 0.0075, \theta_\gamma = -3.0$.

M	Akbar et al.[27]	Bilal et al.[28]	Present study
0.0	− 1.0	− 1.0	− 1.0
0.5	− 1.11803	− 1.11800	− 1.11796
1.0	− 1.41419	− 1.41421	− 1.41421

Table 3. Validation of study with already publisded works[27,28] when $We = 0, \beta = 0, \lambda_1 = 0$.

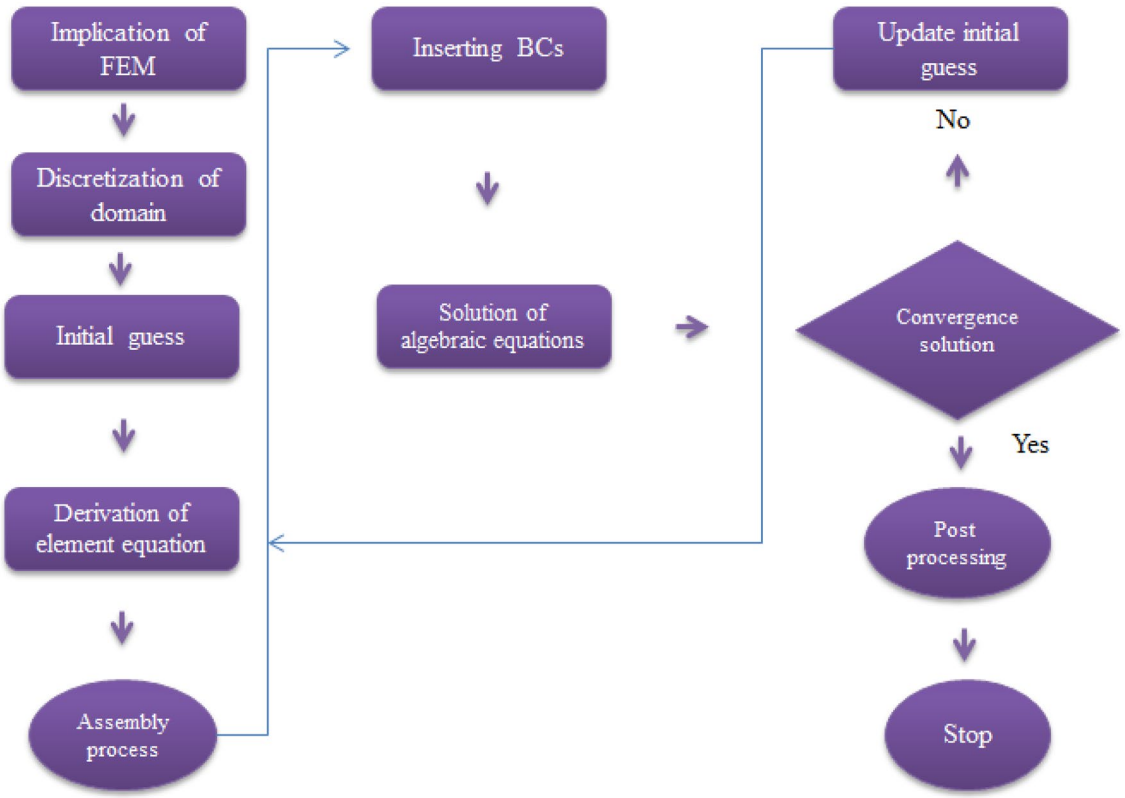

Figure 2. Flow chart of FEM.

- Complex geometric problems can be handled by FEM;
- Most of arising problems in applied science are resolved by FEM;
- It deals with different types of boundary conditions;
- Relatively required low investment, time and resources;
- It behaves significantly well in view of discretization of derivatives.

Residuals. The resiudulas[2] of desired problem are

$$\int_{\eta_e}^{\eta_{e+1}} w_1\left(F'-H\right)d\eta=0, \tag{17}$$

$$\int_{\eta_e}^{\eta_{e+1}} w_2\left[\begin{array}{c} H''+\frac{(d+1)(n-1)}{d}We^d H''(H')^d+\frac{\nu_f}{\nu_{hybrid}}\left(FH'-H^2\right) \\ +\frac{\nu_f}{\nu_{hybrid}}\lambda_1\theta+\frac{\omega exp}{A_1}(-\eta\beta)\end{array}\right]d\eta=0, \tag{18}$$

$$\int_{\eta_e}^{\eta_{e+1}} w_3\left[\begin{array}{c}(1+\epsilon_1\theta)\theta''+\epsilon_1\left(\theta'\right)^2-\beta_a Pr\frac{k_f(\rho C_p)_{hybrid}}{k_{hybrid}(\rho C_p)_f}\left(FH\theta'+F^2\theta''+H_tF\theta'\right) \\ +\frac{k_f}{k_{hybrid}}PrH_t\theta+\frac{k_f(\rho C_p)_{hybrid}}{k_{hybrid}(\rho C_p)_f}PrF\theta'\end{array}\right]d\eta=0, \tag{19}$$

Weak forms. The weak forms are developed using residual method. Shape function[2] is

$$\psi_j=(-1)^{j-1}\left(\frac{-\eta+\eta_{j-1}}{-\eta_j+\eta_{j+1}}\right), i=1,2. \tag{20}$$

Approximations of Galerkin. Stiffness matrices[2] are

$$K_{ij}^{14}=0, K_{ij}^{11}=\int_{\eta_e}^{\eta_{e+1}}\left(\frac{d\psi_j}{d\eta}\psi_i\right)d\eta, K_{ij}^{12}=\int_{\eta_e}^{\eta_{e+1}}\left(\psi_j\psi_i\right)d\eta, B_i^1=0, K_{ij}^{13}=0, B_i^2=0, \tag{21}$$

$$K_{ij}^{22}=\int_{\eta_e}^{\eta_{e+1}}\left[\begin{array}{c}-\frac{d\psi_i}{d\eta}\frac{d\psi_j}{d\eta}-\frac{(d+1)(n-1)}{d}We^d\left(\overline{H}\right)^d\frac{d\psi_i}{d\eta}\frac{d\psi_j}{d\eta}+\frac{\nu_f}{\nu_{hybrid}}\left(\overline{F}\psi_i\frac{d\psi_j}{d\eta}\right) \\ -\frac{\nu_f}{\nu_{hybrid}}\overline{H}\psi_i\psi_j\end{array}\right]d\eta, B_i^2=0, \tag{22}$$

$$K_{ij}^{23}=\left[\frac{\nu_f}{\nu_{hybrid}}\lambda_1\psi_i\psi_j\right]d\eta, K_{ij}^{24}=\left[\frac{\nu_f}{\nu_{hybrid}}\lambda_1\psi_i\psi_j\right]d\eta, K_{ij}^{31}=0, K_{ij}^{32}=0, K_{ij}^{33}=0. \tag{23}$$

$$K_{ij}^{33}=\int_{\eta_e}^{\eta_{e+1}}\left[\begin{array}{c}\left(1+\epsilon_1\overline{\theta}\right)\frac{d\psi_i}{d\eta}\frac{d\psi_j}{d\eta}+\epsilon_1\left(\overline{\theta'}\right)\psi_i\frac{d\psi_j}{d\eta}-\beta_a Pr\frac{k_f(\rho C_p)_{hybrid}}{k_{hybrid}(\rho C_p)_f}\left(\overline{FH}\right)\psi_i\frac{d\psi_j}{d\eta} \\ -\beta_a Pr\frac{k_f(\rho C_p)_{hybrid}}{k_{hybrid}(\rho C_p)_f}\left(\overline{F^2}\right)\frac{d\psi_i}{d\eta}\frac{d\psi_j}{d\eta}-\beta_a Pr\frac{k_f(\rho C_p)_{hybrid}}{k_{hybrid}(\rho C_p)_f}H_t\overline{F}\psi_i\frac{d\psi_j}{d\eta} \\ +\frac{k_f}{k_{hybrid}}PrH_t\psi_i\psi_j+\frac{k_f(\rho C_p)_{hybrid}}{k_{hybrid}(\rho C_p)_f}Pr\overline{F}\psi_i\frac{d\psi_j}{d\eta}\end{array}\right]d\eta, B_i^1=0. \tag{24}$$

Computational tolerance. The computational tolerance is delivered as

$$\left|\frac{\delta_{i+1}-\delta_i}{\delta^i}\right|<10^{-5}. \tag{25}$$

Estimation of error. Several methods are availbale t define error estimation. Residual based estimation[26] is well known method for total energy norm which can be defined as

$$\|E\|=\left(\sum_{i=1}^{n}\|E\|_i^2\right)^{1/2}, \|E\|_i=\int(\nabla E)(\mathcal{L}E)^T d\Omega. \tag{26}$$

where $E=f-\widehat{f}$ and i reveals individual element. Energy norm can be delivered as

$$e_i=\frac{\|E\|}{\|f\|}\times 100\% \tag{27}$$

Results and its outcomes

The development of flow model regarding rheology of Carreau liquid over Riga heated plated is addressed in the presence of magnetic induction. Heat energy and heat transfer rate are visualized involving non-Fourier's law inserting chemical reaction and heat absorption/heat generation. Three kinds of nanomaterial are inserted in EG. ODEs are simulated by FEM. Graphical results associated with heat energy against various parameters are mentioned below.

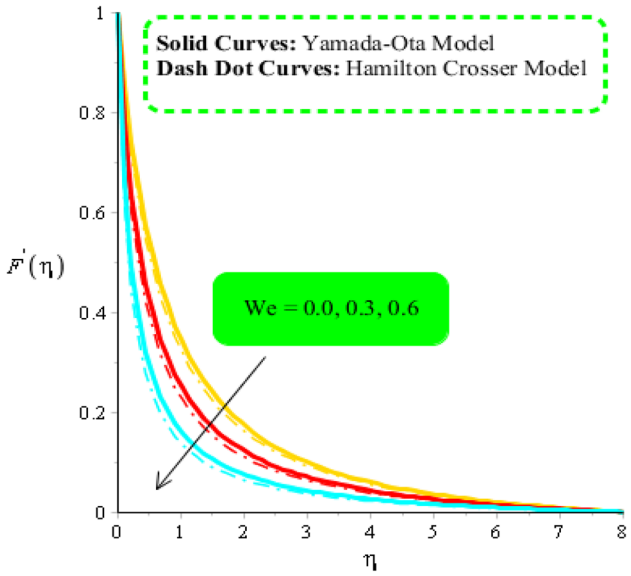

Figure 3. Comparison in velocity field against We when $d = 1, \lambda_1 = 0.3, \beta = 2.0, \epsilon_1 = 1.4, \beta_a = 0.5, Pr = 206, H_t = -2.0, \theta_\gamma = -3.0, \phi_1 = 0.004, \phi_2 = 0.075$.

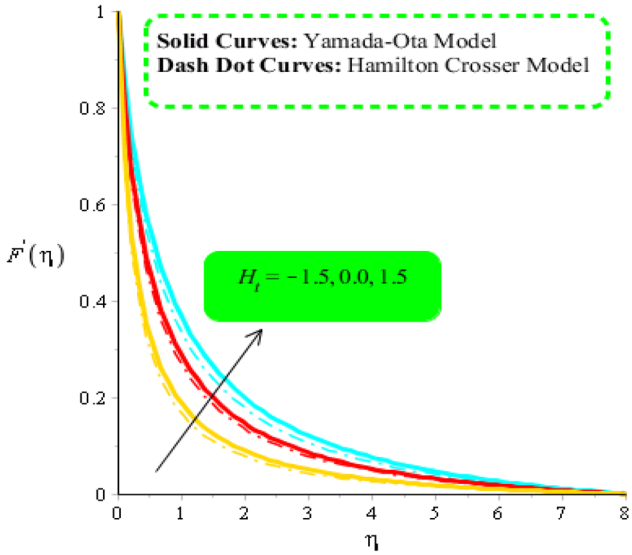

Figure 4. Comparison in velocity field against H_t when $We = 3.0, d = 1, \lambda_1 = 0.3, \beta = 2.0, \epsilon_1 = 1.4, \beta_a = 0.5, Pr = 206, \theta_\gamma = -2.0, \phi_1 = 0.004, \phi_2 = 0.075$.

Comparative outcomes regarding velocity field. Figures 3, 4 and 5 are plotted to measure comparative acceleration among two hybrid fluid models against change in several parameters. It is noticed that model-I is associated with Yamada-Ota hybrid model whereas model-II is considered by Hamilton Crosser hybrid model. Figure 3 is developed to notice relationship between velocity field and We. It predicted that acceleration is decreased slowly when We is enhanced. Physically, it is ratio between viscous force and frictional force. So, fluid becomes significantly viscous due to inverse proportional relation between We and velocity distribution. It is noticed that appearance of We is formulated using rheology of Carreau Yasuda in momentum equations. An inverse relation is visualized among flow and variation of We. Therefore, it can be investigated that fluid becomes thinning when We is enhanced. Further, flow for $We = 0$ is higher than flow for $We \neq 0$. Flow is induced for case of hybrid nanofluid model-I is higher than flow for hybrid nanofluid model-II. An influence of H_t on velocity distribution is carried out by Fig. 4. An implication heat source parameter accelerates maximum heat energy. In this, two types of behavior are addressed in term of heat generation and heat absorption. It is mentioned that heat generation process is occurred for $H_t > 0$ and heat absorption process is occurred for $H_t < 0$. Therefore, flow for $H_t > 0$ is greater than flow for $H_t < 0$. Moreover, fluidic temperature is enhanced when heat generation process is occurred. Physically, an external heat source is utilized to control thickness of momentum boundary

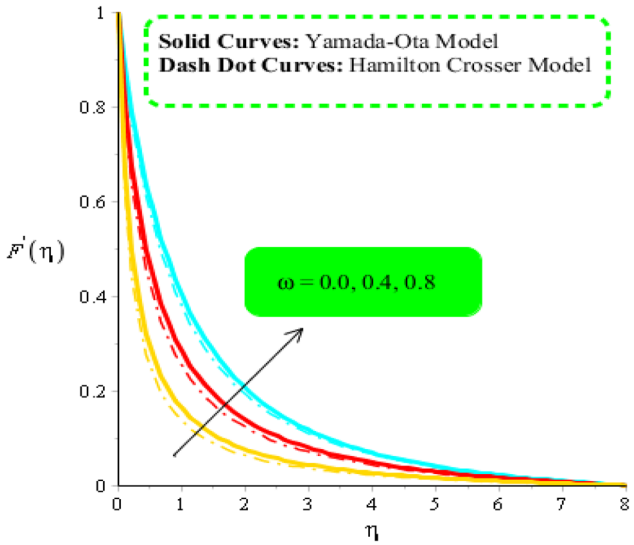

Figure 5. Comparison in velocity field against ω when $We = 3.0, d = 1, \lambda_1 = 0.3, \beta = 2.0, \epsilon_1 = 1.4, \beta_a = 0.5$, $Pr = 206, \theta_\gamma = -3.0, H_t = -2.0, \phi_1 = 0.004, \phi_2 = 0.075$.

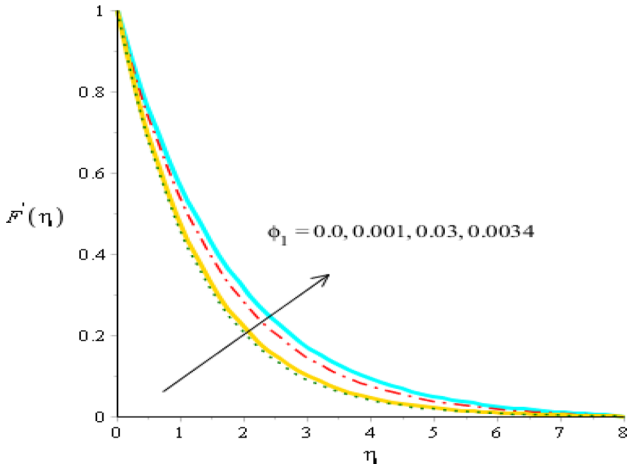

Figure 6. Behavior of velocity field against ϕ_1 when $We = 3.0, d = 1, \lambda_1 = 0.3, \beta = 2.0, \epsilon_1 = 1.4, \beta_a = 0.5$, $Pr = 206, \theta_\gamma = -3.0, H_t = -2.0, \phi_2 = 0.075, \phi_1 = 0.004$.

layers. MBLTs (momentum boundary layer thicknesses) for hybrid nanofluid-I is greater than MBLTs for the case of hybrid nanofluid-II. The role of ω on velocity distribution is carried out by Fig. 5. An acceleration into fluidic particles is augmented when ω is increased. The concept of ω is utilized during process of applying electromagnetic force in Riga plate. It can be noticed that appearance of ω is developed in last term of momentum equation $\frac{\omega exp}{A_1}(-\eta\beta)$. An electromagnetic force is utilized to enhancement flow when ω is increased. Figure 6 reveals effect of ϕ_1 on velocity profile. It is numerically included that motion into particles is enhanced when ϕ_1 is increased. The directly proportional impact for ϕ_1 on flow is investigated in ethylene glycol. Behavior of θ_γ is carried out by Fig. 7. A decreasing trend is visualized on flow behavior when θ_γ is enhanced. It is studied that formulation of θ_γ is established when variable viscosity is addressed in present problem. Higher values of θ_γ are made declination into flow.

Comparative outcomes regarding temperature field. Figures 8, 9 and 10 are developed to estimate variation in temperature field against heat source, ϵ_1 and β_a. Figure 8 reveals increasing behavior of heat energy against change in H_t. Heat energy was enhanced against increment in H_t. This is happened when external heat source is utilized. It is noticed that heat generation process is occurred for $H_t > 0$ and heat absorption process is occurred for $H_t < 0$. Therefore, flow for $H_t > 0$ is greater than flow for $H_t < 0$. Moreover, fluidic temperature is enhanced when heat generation process is occurred. Thermal performance for Yamada Ota model is greater than thermal performance for Hamilton Crosser model. Thermal layer thickness is also increasing function

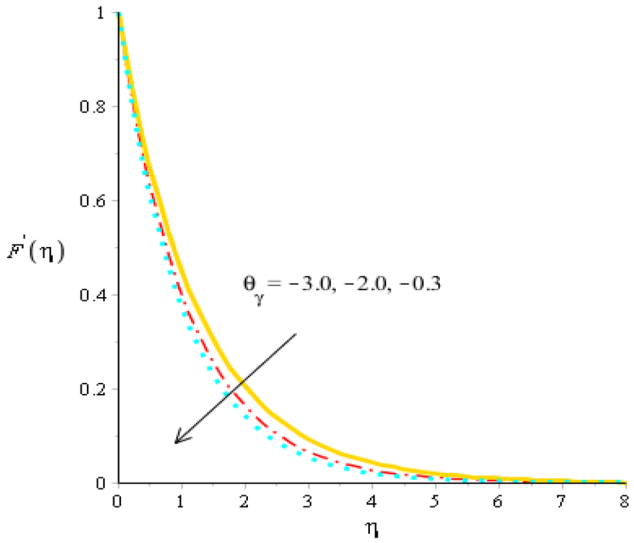

Figure 7. Behavior of velocity field against θ_γ when $We = 2.0, d = 1, \lambda_1 = 0.01, \beta = 4.0, \epsilon_1 = 1.4, \beta_a = 0.05, Pr = 206, H_t = -3.0, \phi_2 = 0.075, \phi_1 = 0.004$.

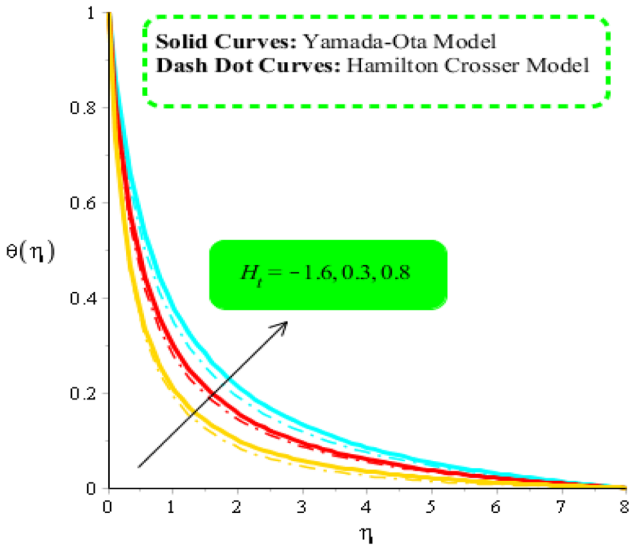

Figure 8. Comparison in temperature field against H_t when $We = 3.0, d = 1, \lambda_1 = 0.3, \beta = 2.0, \epsilon_1 = 1.4, \beta_a = 0.5, \theta_\gamma = -2.0, Pr = 206, \phi_1 = 0.004, \phi_2 = 0.075$.

when H_t is enhanced. Figure 9 captures an estimation of heat energy against variation in β_a. It is investigated that β_a is developed using concept of CCHFM (Cattaneo-Christov heat flux model) in energy and concentration equations. Time relaxation parameter restores maximum heat energy among fluidic particles. Therefore, heat energy is enhanced when β_a is increased. The concept of β_a is produced conspiring non-Fourier's procedure in energy equation as well as in concentration equation. It is utilized to visualized thermal flux among wall and fluid. An enhancement into fluidic temperature is occurred because of direct proportional relation among thermal layers and β_a. Fig. 10 reveals an impact of ϵ_1 on temperature distribution. It is addressed that heat energy is increased against change in ϵ_1. Mathematically, ϵ_2 has directly proportional relation versus mass diffusion rate. From Eq. (7), ϵ_2 is existed in such function (function has domain of temperature). Mass diffusion rate is boosted when ϵ_2 is enhanced. Mass diffusion for $\epsilon_2 = 0$ is less than for the case of $\epsilon_2 \neq 0$. Basically, Therefore, heat energy is inclined. TBLT (thermal boundary layer thickness) for Yamada Ota model is higher than TBLT for the case Hamilton Crosser model. Figure 11 is plotted to measure heat energy versus impact of ϕ_2. It is visualized that heat energy is boosted when ϕ_2 is increased. This is because ϕ_2 is appeared due to occurrence of hybrid nanoparticles (TiO_2/SiO_2) in base fluid named as ethylene glycol. Thermal energy can be boosted by adding an increment of ϕ_2 into particles. Figure 12 reveals effect of θ_γ on temperature profile. Reduction into fluidic heat energy is investigated by considering higher values of θ_γ. It is happened due to appearance of variable viscosity.

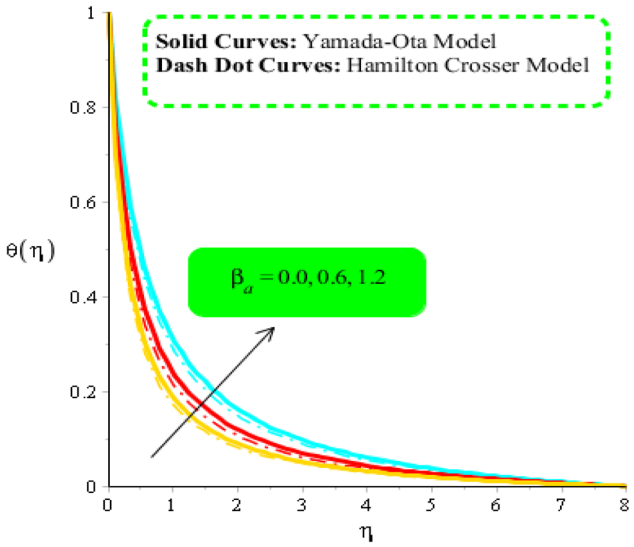

Figure 9. Comparison in temperature field against β_a when $We = 3.0, d = 1, \lambda_1 = 0.3, \beta = 2.0, \epsilon_1 = 1.4, \beta_a = 0.5, Pr = 206, \theta_\gamma = -3.0, H_t = -2.0, \phi_1 = 0.004, \phi_2 = 0.075$.

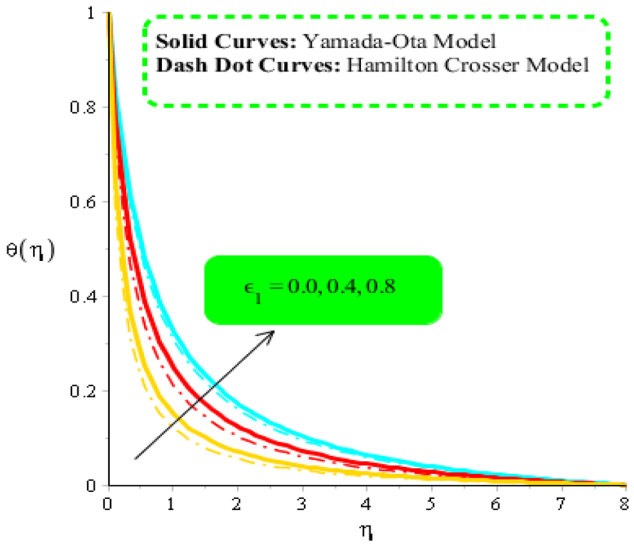

Figure 10. Comparison in temperature field against ϵ_1 when $We = 3.0, d = 1, \lambda_1 = 0.3, \beta = 2.0, \beta_a = 0.5, Pr = 206, \theta_\gamma = -3.0, H_t = -2.0, \phi_1 = 0.004, \phi_2 = 0.075$.

An estimation regarding wall stress and temperature gradient. Table 4 is prepared to measure consequences of We, H_t and ϵ_1 on wall stress and heat energy rate. It is estimated that divergent velocity and heat energy rate are declined versus the change in H_t. But divergent velocity is enhanced versus the change in We. These outcomes are recorded in Table 4. Table 5 demonstrates impact of heat transfer rate against variation in Pr, β_a and λ_1. From Table 5, it is included that thermal performance of heat transfer rate is significantly decreased when Pr, β_a and λ_1 are enhanced. The outcomes regarding heat transfer rate are recommended in Table 5.

Main findings

The numerical investigation has been performed to discuss the contribution of nanoparticles for the thermal enhancement in Carreau Yasuda liquid past over a Riga plate in the presence of variable properties. The derived equations are tackled numerically and important findings are reported as

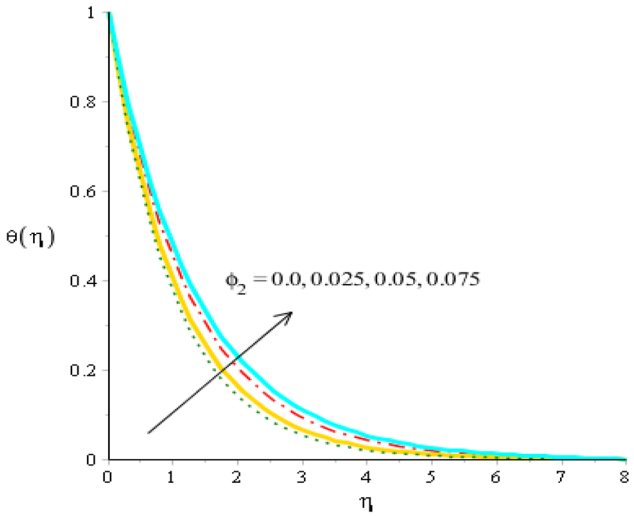

Figure 11. Comparison in temperature field against ϕ_2 when $We = 3.0, d = 1, \lambda_1 = 0.3, \beta = 2.0, \beta_a = 0.5$, $Pr = 206, \theta_\gamma = -3.0, H_t = -2.0, \phi_1 = 0.004$.

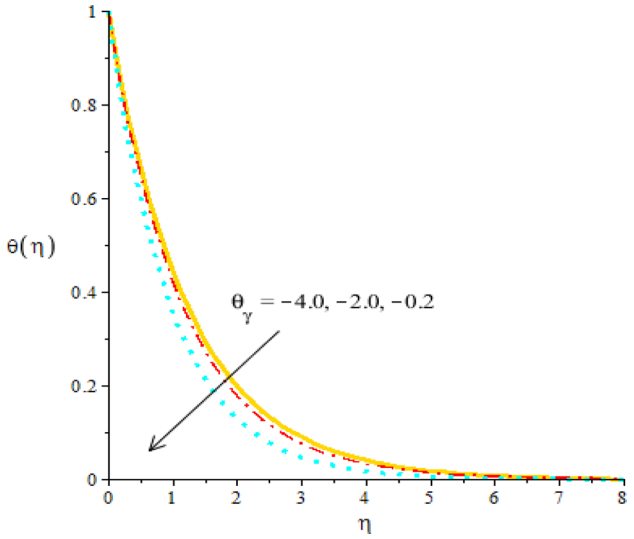

Figure 12. Behavior of temperature field against θ_γ when $We = 4.0, d = 0.3, \lambda_1 = 0.1, \beta = 2.0, \beta_a = 0.04$, $Pr = 206, H_t = -4.0, \phi_1 = 0.004, \phi_2 = 0.075$.

- Augmenting values of *We* increase the dimensionless stress at boundary but depreciate the mass and heat transfer rates;
- Maximum performance of heat energy rate can be achieved with source of hybrid nanoparticles as applicable in coolants related to automobiles, dynamics of fuel, pharmaceutical processes, vehicle thermal adjustment, cooling process, microelectronics, temperature enhancement and temperature reduction;
- Comparative study have been performed to ensure the authenticity of solution;
- Convergence analysis has been shown through grid independent analysis and three hundred elements are taken to establish the convergence;
- The present problem related to electro-magneto-hydrodynamic has applicable in micro coolers, fluidic network flow, fluidic chromatography and thermal reactors.

Variation in parameters	$-Re^{1/2}Cf$	$-Re^{-\frac{1}{2}}NU$
WE		
0.0	0.04083083709	0.8718781018
0.4	0.04115641821	0.7608320013
0.8	0.04548199932	0.5334280014
H_t		
− 1.5	0.05842070236	0.6865965216
0.0	0.02884959667	1.023554468
0.5	0.01075945969	1.268425453
ϵ_1		
0.0	0.02606740874	2.133026234
0.3	0.03568914202	0.687196814
0.5	0.1784160787	0.169312154

Table 4. Simulations of divergent velocity (wall stress), Nusselt number and mass diffusion rate against ϵ_1, H_t and We.

Variation in parameters	$-Re^{-\frac{1}{2}}Nu$
Pr	
203	0.37123950368
205	0.33066012203
206	0.31062012239
λ_1	
0.0	0.96120133102
0.6	0.81663202181
0.9	0.76023217182
β_a	
0.0	0.52322106912
2.0	0.42205522643
3.0	0.2245533610

Table 5. Simulations of Nusselt number rate against Pr, λ_1 and β_a when $We = 3.0, d = 1, \lambda_1 = 0.3, \beta = 2.0$, $\epsilon_1 = 1.4, \phi_1 = 0.004, \phi_2 = 0.075, H_t = -3.0$.

Data availability

The datasets used and/or analysed during the current study available from the corresponding author on reasonable request.

Received: 10 June 2022; Accepted: 17 October 2022
Published online: 08 November 2022

References

1. Reddy, S. R. R., Raju, C. S. K., Gunakala, S. R., Basha, H. T. & Yook, S. J. Bio-magnetic pulsatile CuO–Fe3O4 hybrid nanofluid flow in a vertical irregular channel in a suspension of body acceleration. *Int. Commun. Heat Mass Transfer* **135**, 106151 (2022).
2. Nazir, U., Saleem, S., Nawaz, M., Sadiq, M. A. & Alderremy, A. A. Study of transport phenomenon in Carreau fluid using Cattaneo-Christov heat flux model with temperature dependent diffusion coefficients. *Phys. A* **554**, 123921 (2020).
3. Xiu, W., Saleem, S., Weera, W., & Nazir, U. Cattaneo-Christove thermal flux in Reiner Philippoff martial under action of variable Lorentz force employing tri-hybrid nanomaterial approach. *Case Stud. Therm. Eng.* 102267 (2022).
4. Dogonchi, A. S., Waqas, M. & Ganji, D. D. Shape effects of Copper-Oxide (CuO) nanoparticles to determine the heat transfer filled in a partially heated rhombus enclosure: CVFEM approach. *Int. Commun. Heat Mass Transfer* **107**, 14–23 (2019).
5. Al-Mdallal, Q., Prasad, V. R., Basha, H. T., Sarris, I. & Akkurt, N. Keller box simulation of magnetic pseudoplastic nano-polymer coating flow over a circular cylinder with entropy optimisation. *Comput. Math. Appl.* **118**, 132–158 (2022).
6. Basha, H.T., Rajagopal, K., Ahammad, N.A., Sathish, S., & Gunakala, S.R. Finite Difference computation of Au-Cu/magneto-bio-hybrid nanofluid flow in an inclined uneven stenosis artery. *Complexity* (2022).
7. Reddy, S.R.R., Basha, H.T., & Duraisamy, P. Entropy generation for peristaltic flow of gold-blood nanofluid driven by electrokinetic force in a microchannel. *Eur. Phys. J. Spec. Top*. 1–15 (2022).
8. Basha, H. T. & Sivaraj, R. Entropy generation of peristaltic Eyring-Powell nanofluid flow in a vertical divergent channel for biomedical applications. *Proc. Inst. Mech. Eng. Part E J. Process Mech. Eng.* **235**(5), 1575–1586 (2021).
9. Anantha Kumar, K., Sugunamma, V. & Sandeep, N. Influence of viscous dissipation on MHD flow of micropolar fluid over a slendering stretching surface with modified heat flux model. *J. Therm. Anal. Calorim.* **139**(6), 3661–3674 (2020).

10. Anantha Kumar, K., Sugunamma, V. & Sandeep, N. Effect of thermal radiation on MHD Casson fluid flow over an exponentially stretching curved sheet. *J. Therm. Anal. Calorim.* **140**(5), 2377–2385 (2020).
11. Kumar, A., Sugunamma, V. & Sandeep, N. Impact of non-linear radiation on MHD non-aligned stagnation point flow of micropolar fluid over a convective surface. *J. Non-Equilib. Thermodyn.* **43**(4), 327–345 (2018).
12. Sankar, M., Park, Y., Lopez, J. M. & Do, Y. Numerical study of natural convection in a vertical porous annulus with discrete heating. *Int. J. Heat Mass Transf.* **54**(7–8), 1493–1505 (2011).
13. Haneef, M., Nawaz, M., Alharbi, S. O. & Elmasry, Y. Cattaneo-Christov heat flux theory and thermal enhancement in hybrid nano Oldroyd-B rheological fluid in the presence of mass transfer. *Int. Commun. Heat Mass Transfer* **126**, 105344 (2021).
14. Nawaz, M., Arif, U. & Qureshi, I. H. Impact of temperature dependent diffusion coefficients on heat and mass transport in viscoelastic liquid using generalized Fourier theory. *Phys. Scr.* **94**(11), 115206 (2019).
15. Gul, T. *et al.* Exact solution of the two thin film non-Newtonian immiscible fluids on a vertical belt. *J. Basic. Appl. Sci. Res.* **4**(6), 283–288 (2014).
16. Abdelsalam, S. I. & Sohail, M. Numerical approach of variable thermophysical features of dissipated viscous nanofluid comprising gyrotactic micro-organisms. *Pramana* **94**(1), 1–12 (2020).
17. Chu, Y. M., Nazir, U., Sohail, M., Selim, M. M. & Lee, J. R. Enhancement in thermal energy and solute particles using hybrid nanoparticles by engaging activation energy and chemical reaction over a parabolic surface via finite element approach. *Fract. Fract.* **5**(3), 119 (2021).
18. Basha, H. T. & Sivaraj, R. Exploring the heat transfer and entropy generation of Ag/Fe3O4-blood nanofluid flow in a porous tube: a collocation solution. *Eur. Phys. J. E* **44**(3), 1–24 (2021).
19. Alam, M. K. *et al.* Thin film flow of magnetohydrodynamic (MHD) pseudo-plastic fluid on vertical wall. *Appl. Math. Comput.* **245**, 544–556 (2014).
20. Sohail, M. *et al.* Utilization of updated version of heat flux model for the radiative flow of a non-Newtonian material under Joule heating: OHAM application. *Open Phys.* **19**(1), 100–110 (2021).
21. Sohail, M., & Raza, R. Analysis of radiative magneto nano pseudo-plastic material over three dimensional nonlinear stretched surface with passive control of mass flux and chemically responsive species. *Multidiscip. Model. Mater. Struct*. (2020).
22. Shafiq, A., Khan, I., Rasool, G., Sherif, E. S. M. & Sheikh, A. H. Influence of single-and multi-wall carbon nanotubes on magnetohydrodynamic stagnation point nanofluid flow over variable thicker surface with concave and convex effects. *Mathematics* **8**(1), 104 (2020).
23. Madhukesh, J. K., Varun Kumar, R. S., Punith Gowda, R. J., Prasannakumara, B. C. & Shehzad, S. A. Thermophoretic particle deposition and heat generation analysis of Newtonian nanofluid flow through magnetized Riga plate. *Heat Transfer* **51**(4), 3082–3098 (2022).
24. Sohail, M., Nazir, U., Chu, Y. M., Al-Kouz, W. & Thounthong, P. Bioconvection phenomenon for the boundary layer flow of magnetohydrodynamic Carreau liquid over a heated disk. *Sci. Iran.* **28**(3), 1896–1907 (2021).
25. Gul, H., Ramzan, M., Nisar, K. S., Mohamed, R. N. & Ghazwani, H. A. S. Performance-based comparison of Yamada-Ota and Hamilton-Crosser hybrid nanofluid flow models with magnetic dipole impact past a stretched surface. *Sci. Rep.* **12**(1), 1–11 (2022).
26. Brenner, S.C., Scott, L.R., & Scott, L.R., The mathematical theory of finite element methods (Vol. 3, pp. 263–291) (Springer, New York, 2008).
27. Akbar, N. S., Khan, Z. H., Haq, R. U. & Nadeem, S. Dual solutions in MHD stagnation-point flow of Prandtl fluid impinging on shrinking sheet. *Appl. Math. Mech.* **35**(7), 813–820 (2014).
28. Bilal, S., Rehman, K. U., Malik, M. Y., Hussain, A. & Awais, M. Effect logs of double diffusion on MHD Prandtl nano fluid adjacent to stretching surface by way of numerical approach. *Res. Phys.* **7**, 470–479 (2017).
29. Wakif, A., Boulahia, Z., Amine, A., Animasaun, I.L., Afridi, M.I., Qasimd, M. & Sehaqui, R. Magneto-convection of alumina-water nanofluid within thin horizontal layers using the revised generalized Buongiorno's model. *Front. Heat Mass Transfer (FHMT)*, **12** (2018).
30. Rasool, G. *et al.* Numerical scrutinization of Darcy-Forchheimer relation in convective magnetohydrodynamic nanofluid flow bounded by nonlinear stretching surface in the perspective of heat and mass transfer. *Micromachines* **12**(4), 374 (2021).
31. Rasool, G. *et al.* Significance of Rosseland's radiative process on reactive Maxwell nanofluid flows over an isothermally heated stretching sheet in the presence of Darcy-Forchheimer and Lorentz forces: Towards a new perspective on Buongiorno's model. *Micromachines* **13**(3), 368 (2022).

Author contributions

All the authors reviewed the manuscript and approved the submission.

Funding

This research has received funding support from the NSRF via the Program Management Unit for Human Resources & Institutional Development, Research and Innovation [grant number B05F640204]. Also, this research was supported by the Postdoctoral Researchers Fellowship Training Program from Khon Kaen University, Khon Kaen 40002, Thailand.

Competing interests

The authors declare no competing interests.

Additional information

Correspondence and requests for materials should be addressed to M.S., K.M. or M.R.A.

Reprints and permissions information is available at www.nature.com/reprints.

Publisher's note Springer Nature remains neutral with regard to jurisdictional claims in published maps and institutional affiliations.